J Mater Sci (2006) 41:6655–6672
DOI 10.1007/s10853-006-0203-8

Current research into modelling of shock damage to large scale composite panels

H. E. Johnson · L. A. Louca · S. E. Mouring

Published online: 30 September 2006

Abstract This study aims to model the damage incurred to large woven roving E-glass/vinyl-ester composite panels subjected to shock loads, with particular emphasis on developing an effective, simple to use delamination model. An energy criterion for failure is applied at resin-rich layers, which are modelled in between every ply. The finite element program Abaqus/Explicit together with a user material subroutine (VUMAT) is used to simulate both large and small scale impact tests. The resin-rich layers are modelled as non-linear elastic and matrix and fibre damage is modelled at the woven plies using Hashin's 2D stress-based failure criteria with a once-only degradation of the material properties.

Introduction

The ability to numerically model the damage incurred to composite materials and structures subjected to impulsive loading has become an increasingly important topic in the field of structural engineering. There are a number of approaches for modelling the behaviour of composites under damaging loads but none of the methods are considered universally applicable as they lack robustness. This was concluded by the Worldwide Failure Exercise performed by Hinton [1] where a number of criteria were tested. It is also evident that research into modelling matrix, fibre and in particular, delamination damage in large naval composite structures is limited. Delamination has in the past been largely modelled using either stress based criteria or cohesive zone models. The cohesive zone models are dependent on the energy data from small coupon fracture tests and have so far been limited to modelling only a few delaminating layers in structures that have thus far been relatively small in size. Tang et al. [2] took an engineering approach for the residual analysis of impacted laminated composites and used a bending strain energy density expression for delamination prediction but its implementation is limited to a computer code that was specially developed based on their model features.

A review on delamination predictive methods [3] discusses damage and fracture mechanics approaches applied to low velocity impact events on aircraft composites. They conclude that additional development of these techniques is required before any one technique can be described as a definitive delamination model. Cohesive interface delamination FE models have also been formulated by Espinosa et al. [4] but have been applied to small specimens, using a fine mesh to model the interlaminar fracture process using data from standard fracture tests. Instead, other energy methods have been experimented by Ruiz [5] and Mines et al. [6] who examined the differences in energy density dissipation between specimens for a number of specimen sizes that were subjected to impact up to perforation.

H. E. Johnson (✉) · L. A. Louca
Department of Civil & Environmental Engineering,
Imperial College London, London SW7 2AZ, UK
e-mail: hayley.johnson@imperial.ac.uk

S. E. Mouring
Department of Naval Architecture and Ocean Engineering,
United States Naval Academy, Annapolis, MD 21402, USA

Studies on impact testing and impact modelling of glass-reinforced plastic plates includes that by Sutherland [7] who tested a range of diameter to thickness ratios of circular glass/polyester plates, ranging in size from 100 mm to 200 mm (7.87 in) in diameter. The impact velocity varied up to a maximum of 6.19 m/s. The development of the three damage modes; matrix, fibre and delamination was examined and also the force–displacement and force–time response. A fracture mechanics model was used to describe the onset of delamination and an energy balance approach for modelling the impact force and incident energy. Low velocity impact damage and residual strength of woven fabric glass/polyester laminates was also carried out by Davies and Hitchings [8] who related the impact force and incident kinetic energy to identify damage initiation. The plates were 100–500 mm (3.94–19.68 in) long and up to 25 mm (0.984 in) thick. Damage-force maps were developed from the experiments and proved to be successful with carbon composite plates of different sizes. A simple mode II fracture analysis was used to model a single circular delamination in an isotropic material, with the assumption that the woven fabric is not too far from isotropic. Kuboki et al. [9] carried out impact tests on glass/polyester specimens to search for the relationship between the delamination resistance and the impact resistance. Delamination resistance was characterized using static mode I and mode II delamination tests. Their study highlighted the problems currently existing in the relationship between the delamination resistance of GFRP and its impact resistance. Hou et al. [10] describe an improved stress-based delamination criterion for laminated composite structures and verified with low velocity impact tests on plates $140 \times 85 \times 2.6$ mm ($5.51 \times 3.35 \times 0.1$ in) The failure criteria were implemented in LS-DYNA3D using one solid element through the thickness and taking into consideration the out-of-plane stresses for damage initiation. The influence of matrix cracking and fibre failure on delamination was modelled by reducing the interlaminar shear strength. Reis and Freitas [11] determined through experiment the limit loading capacity and damage growth mechanisms of impacted composite laminates when subjected to compression after impact (CAI) loading. They concluded that the residual strength is influenced by the delaminated area, which is a function of the impact energy.

It is well known that woven-fabric/polymer composites demonstrate a substantial amount of inelastic behaviour, which often occurs during the initial loading stages of the material, however some of the load paths create more non-linearity than others. Johnson and Simon [12] modelled the elastic and inelastic behaviour of 0.25×0.25 m glass fabric/epoxy plates using damage mechanics and a plastic potential function that is a function of the in-plane shear stress only. Other authors have also made the assumption that the fibre direction behaves largely in an elastic manner [13] unlike the resin-dominated directions.

Despite this, tests on some woven composites have shown that the strength and elastic modulus in the fibre directions is sensitive to strain rate, as concluded by Khan and Huang [14] who carried out tests on WR E-glass/Derakane 8084 vinyl-ester composites, mainly used in naval applications, for strain rates of 10^{-3}–10 s^{-1}. They also found that the strength in the through-thickness direction did increase whereas the modulus change was insignificant. Strain rate modelling is thus important when it comes to obtaining the stresses and strains. However, depending on the delamination model employed, the significance of the strain rate on the delamination prediction may vary.

This study aims to propose an approach for modelling matrix, fibre and delamination damage using test data from full and small scale impact tests and high strain rate tensile and compression tests through the thickness. The experimental data comes from a composite that is used predominantly in naval applications; a woven roving E-glass/Derakane 8084 vinyl-ester composite manufactured by an advanced Vacuum Assisted Resin Transfer Moulding (VARTM) technique called ''CARTM'' (Channel Assisted Resin Transfer Moulding). The composite has a 55–70% fibre volume fraction and a low void volume fraction resulting from a superior consolidation of the fibres and matrix produced by the CARTM process. The material properties are shown in Table 1.

The main concern in this study is to model the underlying delamination damage at the interlaminar

Table 1 Average material properties taken from a range of coupon test results for the E-glass/Derakane 8084 vinyl-ester composite, made by VARTM

E11 (Gpa)	E22 (Gpa)	E12 (Gpa)	S13 (Mpa)	S23 (Mpa)
24.139	24.139	8.273	51.6	51.6
E13 (Gpa)	E23 (Gpa)	$S11_T$ (warp) (Mpa)	$S22_T$ (fill) (Mpa)	$S11_c = S22_c$ (Mpa)
3.585	3.585	330.328	298.6	329.6

regions. A simple energy approach is used to model delamination and Hashin's 2D stress criterion to model matrix and fibre failure. The energy criterion for delamination is applied at the resin-rich layers (RR-layers), these being a resin-rich region that is naturally present in between every ply in composite materials and it is at these locations that delaminations are most likely to occur. Although the use of RR-layers is still a relatively new and under-practiced technique, literature suggests that a maximum transverse shear strain criterion has been previously applied at the RR-layers to model delamination, [15]. Other work includes that by Boh et al. [16] who applied a maximum stress criterion at these layers in modelling the response of woven composite beams subjected to transverse shear loading.

Delamination is a very prominent failure mode for shock damaged composites and should ideally be modelled using full-scale test data to minimize any scaling uncertainties. For low velocity impacts the delamination and matrix damage area is proportional to the impact energy, [15]. In order to validate the numerical model, both large and small scale panels, have been shocked under impact as part of a wider study to establish the residual strength of the panels under in-plane compression loading. The sensitivity of the results to two modelling variables is examined, particularly with respect to the transverse stress predictions.

Impact shock modelling

FE analyses are carried out in Abaqus/Explicit to model the low velocity impact of two different sized plates in order to calibrate the models at different scales. The large scale panel measures $1.524 \times 1.524 \times 0.0381$ m (5×5 ft $\times$ 1.5 in) and the small scale panels are $0.2286 \times 0.1778 \times 0.00638$ m ($9 \times 7 \times 0.25$ in).

In order to incur the kind of damage that would be produced by a vessel impacting debris at sea (such as logs) under a speed of up to 10 knots, (5.1 m/s) the impactor must be heavy, of large diameter and travel at a low velocity. A schematic of the large panel test fixture is shown in Fig. 1. Following smaller impact trials, the tup mass was chosen as 453 kg (1,000 lbs), the tup diameter 203.2 mm (8 in) and the tup velocity 4.6 m/s (15 ft/s).

Strain rate tests on vinyl-ester composites have indicated an increase in modulus and strength values over those from quasi-static tests, [17]. Strain rate tests in the warp and fill directions of a SCRIMP manufactured glass/vinyl-ester 510A WR were carried out for strain rates ranging from 0.1 s^{-1} to 5 s^{-1}, [18]. However, the moduli results did show divergence and thus were determined as inconclusive. The ultimate strength results were more promising, seeing an increase in value of 59–82% from static to dynamic at 5 s^{-1}. The only through-thickness strain rate data available was carried out under compres-

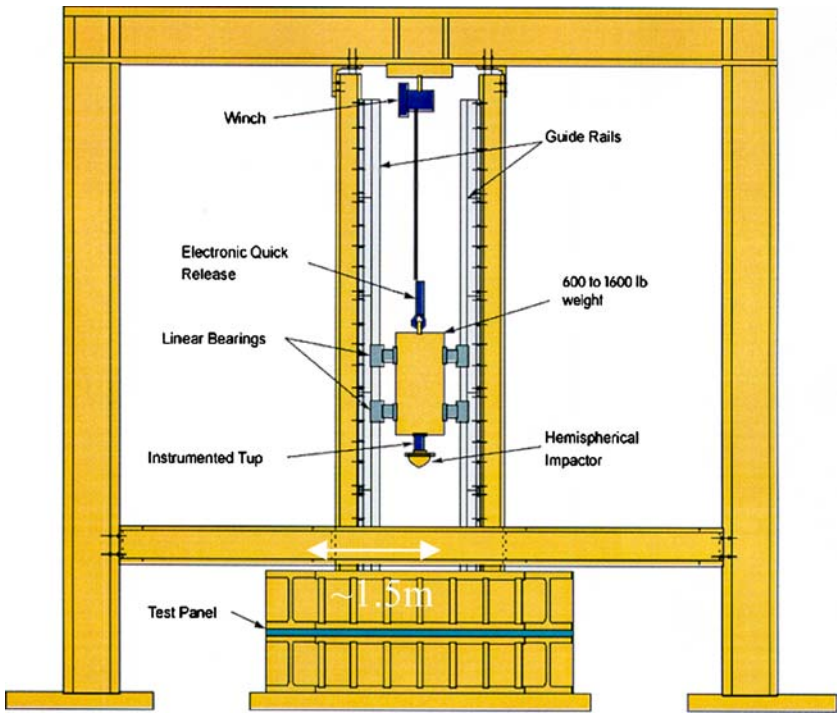

Fig. 1 Schematic of large panel impact test fixture

sion on a hand lay-up glass/Derakane 8084 composite sample obtained from a half-scale Corvette, subjected to strain rates of 0.001 s^{-1} and 100 s^{-1}. The composite was poorly consolidated, giving results that are smaller than what was obtained under quasi-static loading for a very similar resin, a Derakane 510A. The compression and tension results for this composite are shown in Table 2. The table shows the average values from five specimens from five different Derakane 510A batches. This composite had typical fibre volume fractions (FVF) of between 50% and 55%, and although this is not very high, the material was better consolidated through the SCRIMP process than the hand lay-up composite.

As the impact testing may see strain rates of over 100 s^{-1} and based on what we know about the effects of increasing the strain rate, the through-thickness modulus used in the FE analyses is taken as the largest value from the available tests and that is the compressive value from the quasi-static tests for the SCRIMP material in Table 2.

A User Material subroutine (VUMAT) is needed for all the Abaqus/Explicit analyses if failure criteria are to be defined, forcing the user to also define the composite's constitutive behaviour. In contrast, Abaqus/Standard allows the option of using a specific User Defined Field subroutine (USDFLD) that allows state dependent variables and user defined fields to describe the failure criteria, omitting the need to write the constitutive equations.

Table 2 Through-thickness tensile and compressive strengths and moduli taken from five panels fabricated from E-glass and Dow D

Material	Average ultimate strength/10^6 N/m^2	Average modulus of elasticity/ 10^9 N/m^2
Resin Batch 1	Tens.: 35.43	Tens.: 10.27
Panel #1	STD = 2.4	
FVF = 52.3%	Comp.: 541.55	Comp.: 12.44
	STD = 21.11	
Resin Batch 2	Tens.: 33.95	Tens.: 12.08
Panel #2	STD = 2.97	
FVF = 53.9%	Comp.: 563.78	Comp.: 14.08
	STD = 28.19	
Resin Batch 3	Tens.: 21.36	Tens.: 11.17
Panel #3	STD = 2.59	
FVF = 51.8%	Comp.: 547.41	Comp.: 13.62
	STD = 36.67	
Resin Batch 4	Tens.: 39.66	Tens.: 11.08
Panel #4	STD = 2.06	
FVF = 53.8%	Comp.: 547.18	Comp.: 14.46
	STD = 9.18	
Resin Batch 5	Tens.: 22.17	Tens.: 12.66
Panel #5	STD = 1.9	
FVF = 55.3%	Comp.: 591.71	Comp.: 17.65
	STD = 12.47	

For all of the analyses in this study the RR-layers and the woven plies are modelled an elastic materials that are also elastic damaging. The composite woven plies are orthotropic, and Hashin's 2D failure criteria are applied at these layers to model matrix and fibre failure. When failure is depicted, the relevant material properties are degraded to 90% of their original value. The transverse shear stiffness and the through-thickness modulus and Poisson's ratio is only made available in the input file and cannot be modified during the analysis. Delamination damage is modelled with RR-layers, as shown in Fig. 2. The RR-layers are modelled as a fraction of the woven ply thickness, typically 5%, reducing the woven layer thickness accordingly to keep the overall laminate thickness constant.

Two types of RR-layer models are examined with the large plate impact simulations. The first model applies a simple in-plane stress criterion at the RR-layers, ''stress criterion 1'', shown in Eq. 1, with the criteria that failure occurs when RRL1 + RRL2 ≥ 1, at which point all the properties of the resin are degraded to nearly zero. A variation of stress criterion 1 is ''stress criterion 2'', here also evaluated, indicating failure when the largest of either RRL1 or RRL2 is equal or greater than one. The maximum strength values of the resin used in the equations are also reduced to half their value if either matrix or fibre failure is detected first using Hashin's 2D failure criteria, shown with Eq. 2. The strength of the resin in the two in-plane directions x and y, is denoted by X_R^C and Y_R^C for compression and X_R^T and Y_R^T for tension.

The second RR-layer model is to apply a simple internal energy failure criterion at the resin-rich layers. Two energy density values are compared: the average critical energy density value obtained from typical Mode I fracture tests, see Eq. 4, and an energy density criterion from full impact tests.

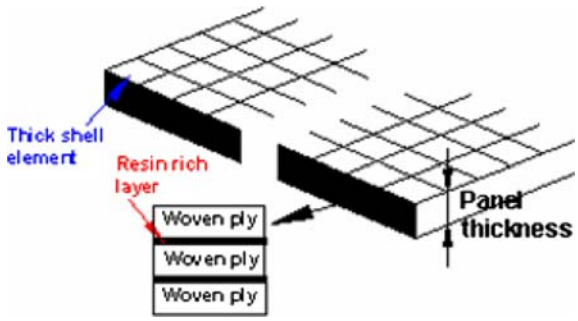

Fig. 2 Composite layering through the thickness of the elements

$$\begin{aligned}
&\text{If } \sigma_{11}<0 \quad \text{then} \quad \text{RRL1} = \left(\frac{\sigma_{11}^{C}}{X_R^{C}}\right)^2 \\
&\text{If } \sigma_{11}>0 \quad \text{then} \quad \text{RRL1} = \left(\frac{\sigma_{11}^{T}}{X_R^{T}}\right)^2 \\
&\text{If } \sigma_{22}<0 \quad \text{then} \quad \text{RRL2} = \left(\frac{\sigma_{22}^{C}}{Y_R^{C}}\right)^2 \\
&\text{If } \sigma_{22}>0 \quad \text{then} \quad \text{RRL2} = \left(\frac{\sigma_{22}^{C}}{Y_R^{T}}\right)^2
\end{aligned} \tag{1}$$

Stress criterion 1:
RR-layer integration point failure if
RRL1 + RRL2 ≥ 1
Stress criterion 2:
RR-layer integration point failure if
RRL1 or RRL2 ≥ 1

$$\left(\frac{\sigma_{11}}{X_T}\right)^2+\left(\frac{\sigma_{12}}{S_{12}}\right)^2 \geq 1$$

Hashin's fibre tension failure

$$\left(\frac{\sigma_{11}}{X_C}\right)^2 \geq 1$$

Hashin's fibre compression failure

$$\left(\frac{\sigma_{22}}{Y_T}\right)^2+\left(\frac{\sigma_{12}}{S_{12}}\right)^2 \geq 1 \tag{2}$$

Hashin's matrix tension failure

$$\frac{\sigma_{22}}{Y_C}\left[\left(\frac{Y_C}{2S_{12}}\right)^2-1\right]+\left(\frac{\sigma_{22}}{2S_{12}}\right)^2+\left(\frac{\sigma_{12}}{S_{12}}\right)^2 \geq 1$$

Hashin's matrix compression failure

The internal energy per unit mass is calculated at every RR-layer integration point using Eq. 3, see Fig. 3. When using shell elements, the transverse stresses are not fed into the subroutine therefore only in-plane stresses are used in this equation. This energy value is updated at the end of every time increment and is compared with the critical energy for failure. V_e is the volume of the resin layer for one element width and ρ is the density of the resin.

$$E_{\text{int}} = \frac{1}{\rho V_e}\int_{V_e}\frac{1}{2}\{\varepsilon\}^T[E]\{\varepsilon\}\partial V = \frac{1}{2\rho}[\sigma]\{\varepsilon\} \tag{3}$$

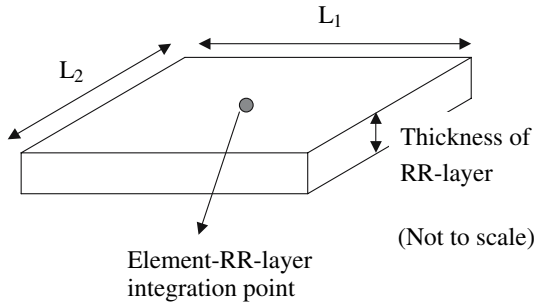

Fig. 3 Showing one of the 49 resin-rich layers within an element

The energy values from the critical fracture tests on the WR E-glass/Derakane 8084 vinyl-ester is shown in Table 3, calculated using Eq. 4, where "R" is the thickness of the RR-layer.

$$E_{\text{frac}} = \frac{L_1 L_2 G_c}{M_{\text{el}}} = \frac{L_1 L_2 G_c}{\rho L_1 L_2 R} = \frac{G_c}{\rho R} \tag{4}$$

The energy value for failure from the impact tests has been obtained from a simple expression, Eq. 5, for the total energy absorbed during impact.

$$E = \int_{t_0}^{t_f} P v \partial t \tag{5}$$

where P and v are the instantaneous load and velocity, respectively, t_0 is the time of initial impact, taken as zero, and t_f is the time at which contact with the plate is lost. Because the instantaneous velocity can only be measured at the beginning and at the end of the impact, the *apparent energy* can be used instead, as shown with Eq. 6.

$$E_a = v_0 \int_0^{t_f} P \partial t \tag{6}$$

This energy for failure is then divided by the mass of the plate to give an energy value that compares with the internal energy calculated at each integration point.

In these impact tests, the contact force is known from experiment and is used in the apparent energy

Table 3 Mode I critical fracture energy test values for WR E-glass/Derakane 8084 vinyl-ester

Crack initiation	Crack propagation
Min value: 3.4 in-lb/in^2 (596 J/m^2)	Min value: 9.05 in-lb/in^2 (1665 J/m^2)
Max value: 4.6 in-lb/in^2 (806 J/m^2)	Max value: 11 in-lb/in^2 (1928 J/m^2)

equation. Where the contact force and time to impact is unknown, an independent energy formulation is required. The ideal is to obtain a critical energy value based on the kinetic energy of the tup, which can be applied to a range of plate sizes. The information on the tup mass and impact velocity is more readily available than the contact force and it would be beneficial that the FE model could incorporate this. If the impulsive event comes from a shock wave, such as from an underwater blast, then the blast pressure would be the most likely data resource. Knowing the blast pressure, Eq. 6 would then be an appropriate equation to use, where P is the blast pressure.

For both RR-layer models, the resin properties at the integration points are degraded to nearly zero when the failure criteria are met. A small residual is retained for numerical stability.

Ideally, to eliminate mesh sensitivity in the numerical analyses would require enforcing a constant mesh resolution over the damage zone. The energy would be calculated for a constant volumetric region that decreases with increase in specimen scale once the relationships are established from experiments between the scale of the specimen and the energy absorbed by the specimen [19]. Unfortunately, Abaqus' VUMAT does not provide element number information into the subroutine and the subroutine is run for every increment at every integration point, for which their locations are also unknown. The effect of mesh density on delamination prediction is later examined with the smaller plate impact simulations.

Large plate impact

The FE simulation results for the large panel are shown for a single mesh density of 44×44 elements and one element through the thickness. This panel is modelled with 50 composite orthotropic (woven) plies and 49 RR-layers.

The implicit analyses are carried out here using standard thick shell elements, S4R, whereas Abaqus's SC8R continuum shell elements are tested in the Explicit analyses. Both shell element types can model the change in shell thickness and enforce plane-stress conditions, however the S4R use Poisson's ratio to allow the thickness to change as a function of the membrane strains only. The thickness strain is defined in terms of the in-plane strains, as shown with Eq. 7. This equation is then expressed in terms of the equivalent changes in displacement of the element's reference surface, thus providing an expression for the change in the element thickness. In contrast, the continuum shell elements discretise a three-dimensional body giving them advantages over the conventional shells by modelling the through-thickness response of the shell more accurately. The SC8R calculates two strains: the primary strain is the effective thickness strain at the element centre directly from the element nodal displacements. The secondary strain is obtained under plane-stress conditions by specifying the thickness Poisson's ratio and allowing the through-thickness strain to be calculated as a linear function of the membrane strains, as with the ordinary thick shells. These secondary strains are subtracted from the primary strains to give the effective thickness strains. An elastic modulus (E33) is defined under the shell section definition in the Abaqus input file and an effective section Poisson's ratio, making them available during the pre-processing stage of input. The normal stress in the thickness direction is thus obtained using these effective thickness strains and section properties and it is assumed to be constant through the thickness of the element. This average transverse normal section stress can be outputted as SSAVG6 for the shell section; for each element through the thickness. Another advantage of the SC8R over the S4R elements is their superior contact modelling [20].

$$\varepsilon_{33} = \frac{-v}{1-v}(\varepsilon_{11} + \varepsilon_{22}) \tag{7}$$

A summary of some of the Standard and Explicit FE results are shown in Table 4. We can see that the most effective FE results are those obtained using the Explicit analysis, applying the energy criterion at the RR-layers using the energy from full-scale impact tests. The largest maximum o.o.p (out-of-plane) displacement, seen in Fig. 4, is obtained using Abaqus/Implicit and the S4R thick shell elements. This is expected as the thick-shell elements have six degrees of freedom compared to the three displacement degrees of freedom for the continuum shell elements, making them a little more flexible. Plots of the o.o.p displacement at the centre of the panel for the Explicit analysis using SC8R elements is shown in Fig. 5.

In the tests, the force of the impact was measured in two ways, by measuring the force directly using an instrumented tup and by integration of the acceleration of the weight box. Both force results were very close and the values calculated using the accelerometer can be seen in Fig. 6. The maximum tup force compares very well with that obtained by the Explicit analysis using the energy for delamination from the impact tests followed by stress criterion 1. The force is 12% larger than that obtained experimentally as is expected, considering that the numerical model does not phys-

Table 4 Comparing delamination criteria using Abaqus /Implicit and Explicit, where "R" is RR-layer thickness

Delamination criterion	Critical energy value (J/M)	Max. out-of-plane displacement (mm)	Max. area of delamination (m^2)
Abaqus/standard			
1 Maximum stress criterion 2, at RR-layers	N/A	34.5	0.0155
Abaqus/explicit			
1 Maximum stress criterion 1, at RR-layers	N/A	31.7	0.004
2 Energy criterion from fracture tests	12,560 (i.e., 0.361 per R)	31.9	0
3 Energy criterion from full-scale impact tests	340	31.9	0.107
Test		28.7	0.0917

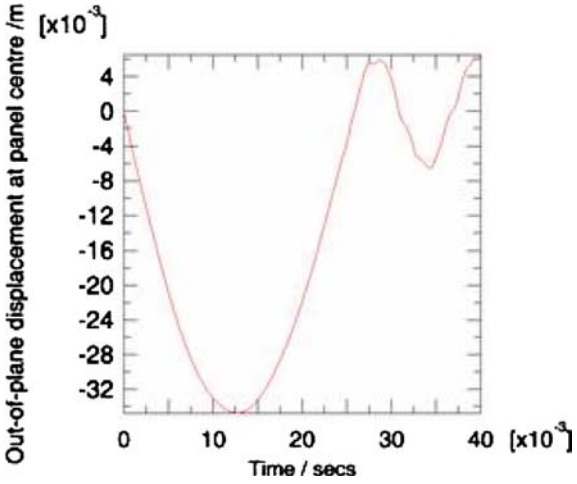

Fig. 4 Out-of-plane displacement at the panel centre (maximum 34.7 mm) using Abaqus/Implicit

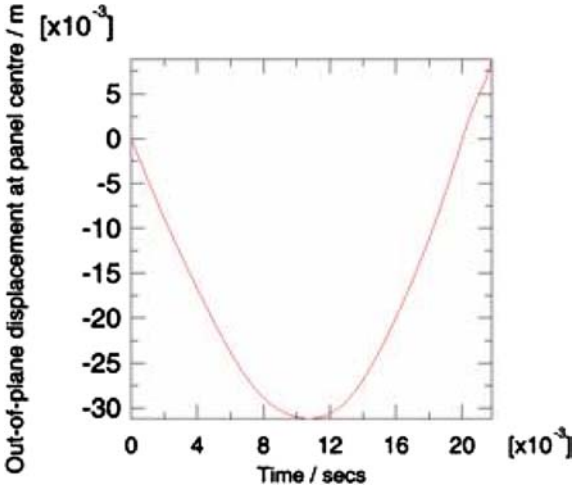

Fig. 5 Out-of-plane displacement at the panel centre (maximum 31.1 mm) using Abaqus/Explicit

ically model the separation of the delaminated layers. Also the frequency content of the load is acceptable and gives some confidence that the damage can at least be captured in a qualitative manner.

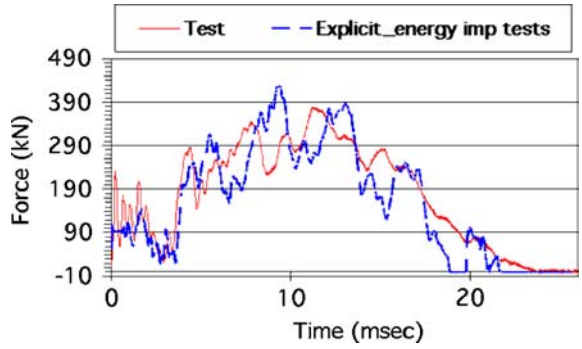

Fig. 6 Impact force at the centre of the panel, FE analyses, Explicit, 44 × 44 elements, stress criterion 1 for delamination

In the numerical simulations it is found that the maximum matrix/fibre damage area is always largest nearest the top and bottom surfaces decreasing in size towards the centre. Delamination damage follows a similar, less symmetrical pattern, with maximum delamination occurring near the bottom face of the panel. In contrast, the tests show delamination all the way through the thickness, more so near the centre of the plate followed by layers near the outer faces. This corroborates the fact that the plate is thick and the transverse stresses will be influential in the delamination process. The maximum bending stresses (responsible for matrix cracking/crushing and an initiator of delamination) together with the normal transverse stresses would have been largely responsible for the delamination found nearer the surfaces. The transverse shear stresses although strongly influential throughout the thickness, are the most responsible for the delamination in the central region of the plate where they are highest (see Fig. 7).

Abaqus/Standard simulation gives a larger matrix and fibre damage area compared to the Explicit analyses; an average of 0.31×0.31 m^2 compared to 0.18×0.18 m^2. The shape of the damage is also dissimilar, attributed to the differences in the two shell

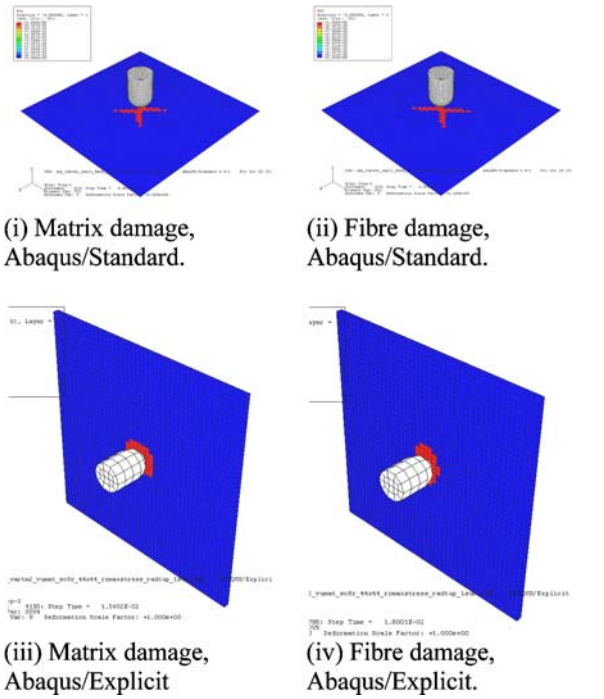

Fig. 7 (**i–iv**) Matrix and fibre damage using the Hashin 2D criteria

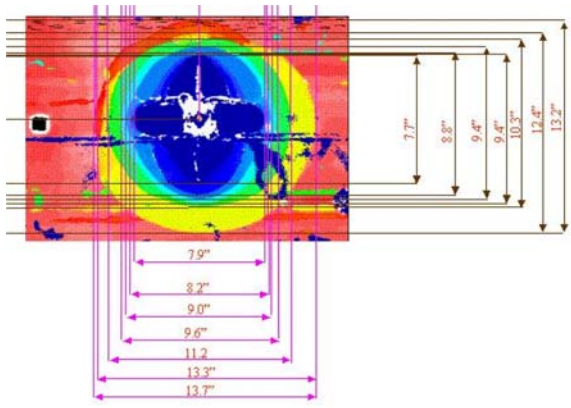

Fig. 8 The variation in colours shows the extent of delamination through the layers for one of the impact tests for a 5 × 5 ft panel. (Damage area in inches, only central portion of plate shown.)

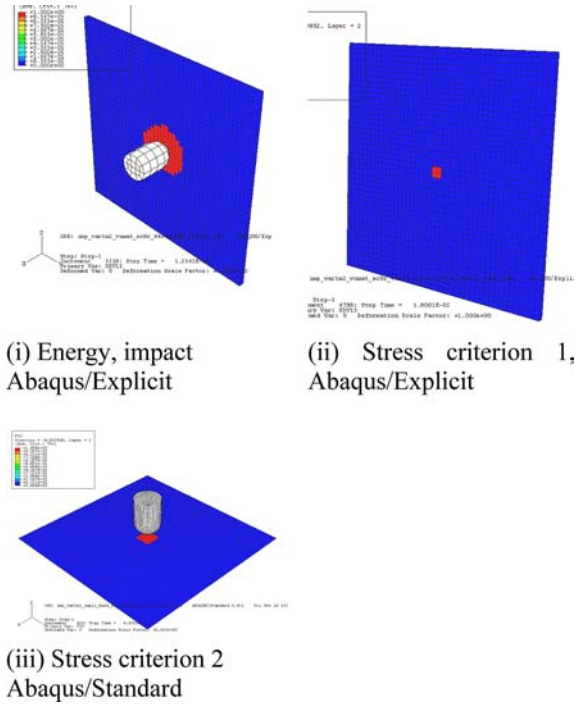

Fig. 9 (**i**), (**ii**) & (**iii**) Showing the extent of delamination produced from the FE analyses

element types. The rectangular shape is generated with the continuum shell largely due to the better contact obtained between the tup and the plate. Conversely, the ordinary shells produce a delamination pattern, which is in the shape of a cross. With all simulations, the maximum matrix damage and fibre damage size falls within the size of the largest delamination area, Fig. 8, and the matrix damage may possibly be somewhat under-predicted.

The *maximum* area of delamination given by the Explicit analysis using the energy from impact tests to model the delamination, compares very closely to that obtained from the test results. Figure 9(i) shows the delamination area at the bottom RR-layer for the FE analysis and Fig. 8 shows the delamination through the thickness from a C-scan for one of the full-scale impact tests. The extent of delamination area obtained near the centre layer is shown with the yellow colouring (the largest shaded area). The maximum delamination is under predicted using the stress based criteria, see Fig. 9(ii) and (iii) and no delamination develops when applying the critical energy for fracture energy values.

Figure 10 shows the delamination through the thickness obtained from the Explicit analysis and the continuum shell elements. The profile demonstrates a larger proportion of the delamination occuring on the bottom face of the panel, reducing to practically zero about one third from the top This distribution of delamination is not correct following the scan results, showing under-predictions at the centre and for the top half of the plate.

Abaqus/Explicit has many advantages over Abaqus/Implicit, including faster run times and no convergence problems, however one of the drawbacks is the large memory usage when using the VUMAT subroutine, namely because of the storage of the state dependent

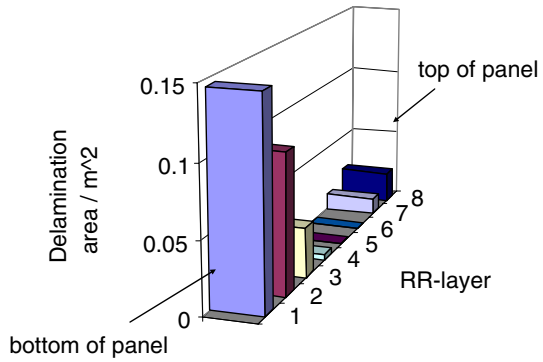

Fig. 10 Delamination through the thickness from Explicit analysis using SC8R elements

variables. However, overall it captures the dynamics of the problem more accurately.

Small plate impact

Composite plates of $0.2286 \times 0.1778 \times 0.00638$ m ($9 \times 7 \times 0.25$ in) were tested under impact. The o.o.p displacement was measured by double integration of the load/time curves obtained from the load cell. Sixteen tests were carried out to see the effect different tup sizes and tup masses have on the o.o.p displacement, contact force and incurred damage. Four of these tests are compared to FE results using SC8R elements in Abaqus/Explicit using a VUMAT. The laminate has nine woven plies and is modelled as an orthotropic material.

The impact velocity is practically the same for the four tests examined, a value of 4.6 m/s. The test results are detailed in Table 5. As with the larger plate simulations, the critical energy for failure criterion obtained from the impact tests is applied to the RR-layers and Hashin's 2d stress based failure criteria is used at the woven plies.

Modelling variables

In this section, all of the following FE analyses are carried out to see the effect of different variables on an FE model of Test 9 (25.4 mm, 18.7 kg tup). Two modelling variables are examined: the mesh density and the number of elements through the thickness. The model "coarse2" has a coarse mesh of $34 \times 44 \times 2$ elements; 34 along the shorter length of the plate and two elements stacked through the thickness. The analysis "Fine2" uses a finer $56 \times 72 \times 2$ element mesh and analysis "Fine9" has $56 \times 72 \times 9$ elements (nine elements through the thickness). Due to the larger number of elements, analysis "Fine9" is carried out using symmetrical boundary conditions on a quarter plate model.

Figure 11 shows the o.o.p displacement obtained for the three different analyses. The surface mesh density has negligible effect on the out-of-plane displacement but the number of elements stacked through the thickness from 2 to 9 does reduce the magnitude of this displacement by about 0.5 mm. The contact force from these analyses is also shown in Fig. 12, showing insignificant differences between them.

The average section normal transverse stress, SSAVG6, can be outputted across the plate for any of the elements. SSAVG6 is largely affected by the mesh density, particularly by the number of elements through the thickness. The variation of SSAVG6 is examined at a location "A" shown in Fig. 13, a distance of approximately 16 mm from the centre of the plate. This location is chosen as it is close to the impact site yet it is not affected by some of the irregularities experience at the contact area between the tup and the plate. Every woven ply and RR-layer has three section points but the SSAVG6 is outputted at the single integration point at the centre of each element.

Increasing the number of elements through the thickness provides a sharper stress output, as each stress is calculated from the strains at the element centre: the more elements the less deviation of the average values from the maximum or minimum across the section. Figure 14 demonstrates how larger and more detailed normal transverse stresses are averaged with nine elements through the thickness compared to two elements through the thickness. The "B" in the legend script refers to the element at the bottom of the plate and "T" the element at the top of the plate. With analysis fine9 there are seven elements also in between. All analyses show that the tensile normal transverse stresses occur on the underside of the plate and the compressive stresses develop on the top side of the plate. The model with nine through-thickness elements estimates that the positive tensile stresses are larger than the negative compressive stresses, whereas the same model with only two through-thickness elements estimates the reverse, although this difference is small. Moreover, the stresses provided by analysis fine9 are of an order of magnitude of up to 50 times larger than those from fine2.

The variation of the transverse normal stress through the thickness h is shown at three increments in time for analysis fine9, see Fig. 15, where z is the distance from the mid-surface of the plate. The maximum tensile SSAVG6 values occur at maximum impact, reducing in value as the tup is close to full separation from the plate, resulting in a smaller difference between the magnitude of the compressive

Table 5 A few test results for the (9 × 7 × 0.25 in) plate

Test	Tup size/mm (inches)	Tup velocity/m/s (ft/s)	Contact Force/kN (lbf)	Mass/kg (lb)	δ/m (in)	Approximate damage size (seen from the top of the plate)/m (in)	Approximate damage size (see from the bottom of the plate)/m (in)	Energy level/J (ft lbf)
1	12.7 (0.5)	4.59 (15.08)	15.15 (3406)	8.55 (18.86)	0.0119 (0.470)	0.0381 × 0.0254 (1.5 × 1)	0.0381 × 0.0381 (1.5 × 1.5)	91.52 (67.5)
2	12.7 (0.5)	4.594 (15.07)	26.98 (6066)	18.62 (41.05)	Penetration	0.0381 × 0.0254 (1.5 × 1)	0.0381 × 0.0381 (1.5 × 1.5)	190.09 (140.2)
3	12.7 (0.5)	4.572 (15)	20.35 (4574)	13.33 (29.39)	0.0141 (0.557)	0.03175 × 0.0254 (1.25 × 1)	0.0381 × 0.0381 (1.5 × 1.5)	140.57 (103.68)
7	25.4 (1)	4.59943 (15.09)	24.64 (5538)	23.69 (52.23)	0.0205 (0.807) (Partial penetration)	0.0381 × 0.0381 (1.5 × 1.5)	0.0508 × 0.0381 (2 × 1.5)	247.59 (182.61)
8	25.4 (1)	4.59638 (15.08)	27.74 (6237)	23.69 (52.23)	0.0186 (0.733) (Partial penetration)	0.03175 × 0.0381 (1.25 × 1.5)	0.04445 × 0.04445 (1.75 × 1.75)	247.59 (182.61)
9	25.4 (1)	4.593 (15.07)	24.93 (5604)	18.70 (41.23)	0.0159 (0.627)	0.03175 × 0.0254 (1.25 × 1)	0.0381 × 0.03175 (1.5 × 1.25)	195.51 (144.2)
12	38.1 (1.5)	4.60553 (15.11)	23.43 (5268)	24.32 (53.61)	0.0223 (0.88)	0.04445 × 0.0381 (1.75 × 1.5)	0.0381 × 0.0381 (1.5 × 1.5)	263.41 (194.28)
13	38.1 (1.5)	4.60858 (15.12)	24.86 (5588)	26.19 (57.73)	0.0229 (0.9)	0.05715 × 0.03175 (2.25 × 1.25)	0.0381 × 0.0381 (1.5 × 1.5)	284.05 (209.5)
15	38.1 (1.5)	6.20878 (20.37)	28.13 (6324)	26.19 (57.73)	0.0376 (1.48)	0.03175 × 0.03175 (2.5 × 1.25)	0.05715 × 0.04445 (2.25 × 1.75)	495.85 (365.72)
16	38.1 (1.5)	7.12927 (23.39)	29.40 (6609)	26.19 (57.73)	0.0546 (2.15)	0.06985 × 0.0508 (2.75 × 2)	0.03175 × 0.03175 (2.5 × 2.5)	

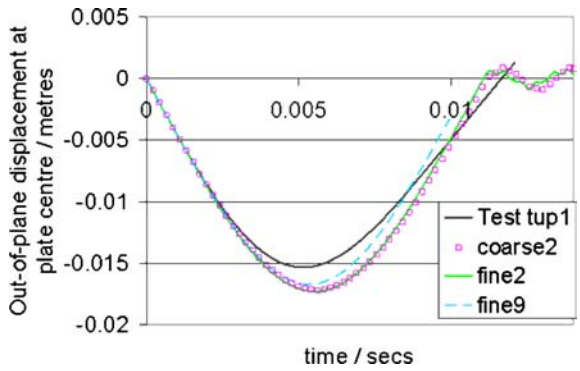

Fig. 11 Maximum o.o.p versus time for FE analyses modelling damage compared to Test 1

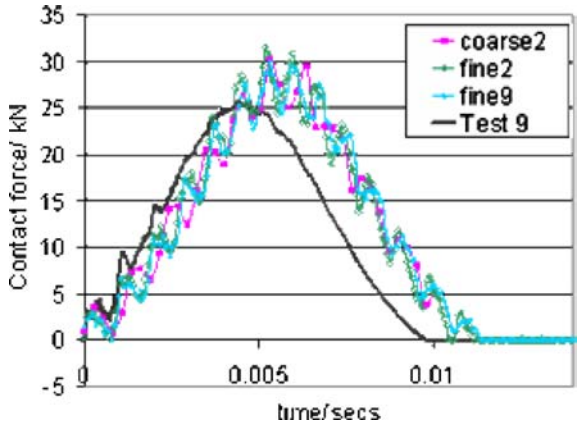

Fig. 12 Contact force versus time—Test 9 and FE simulations of test 9

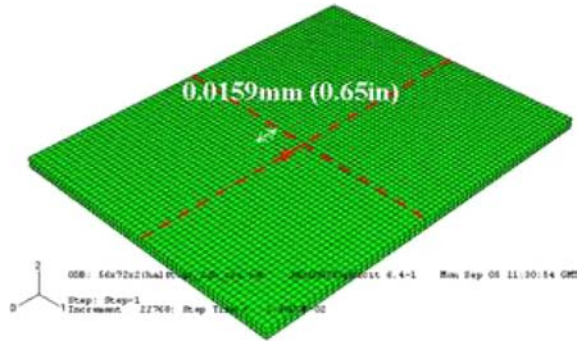

Fig. 13 Location ''A'': approximate location at which SSAVG6 values were taken through the thickness for all the analyses

and tensile values at the top and bottom faces, respectively.

The contours of SSAVG6 for analysis fine9 at the point of maximum o.o.p displacement are shown in Fig. 16. The figure also indicates the stack of elements outlined in red, location A, from which these transverse stress values were outputted for plotting. The element with the maximum tensile normal transverse stress value is at the bottom of the plate where delamination is very pronounced in both the FE simulations and the tests. The high tensile stresses act to pull the plies apart significantly and can cause ''spawling''.

Based on the tensile and compressive through-thickness test data, the analysis with nine through-thickness elements is probably a better approximation of the SSAVG6. We know from experiment that delamination in and around the impact site occurred throughout the plate thickness more so near the lower surface. The largest delaminated area visually inspected from the lower surface in test9 was measured as 0.0381×0.03175 mm (1.5×1.25 in) and the cross-section photo (similar to that shown for test 13 in Fig. 24) shows prominent delamination of the bottom layer. Thus delamination also occurred at location A on this bottom face and would have been initiated by transverse matrix cracks in the adjacent ply resulting from the large bending stresses and developed largely due to the high normal tensile stresses. The maximum SSAVG6 value obtained from analysis fine9 is $350(10^6)$ N/m^2, which exceeds the 21–40 kN quasi-static through-thickness tensile strength values in Table 2 and most likely that also any dynamic values measured in future tests. Thus these predicted tensile SSAVG6 stand-alone values would indicate almost certain delamination at this location.

In test9 delamination is also seen at the top face however the maximum compressive SSAVG6 values predicted in fine9 are of about $75(10^6)$ N/m^2 which is less than the compressive strength values from quasi-static test data shown in Table 2 (giving values of over $500(10^6)$ Nm^2). They are also up to four times smaller than the $400(10^6)$ N/m^2 strength values obtained from the 100 s^{-1} strain rate compressive tests on the Corvette composite hull material. These delaminations are therefore largely propagated by the transverse shear stresses. Matrix crushing of theals top surface e is evident at the centre of the whitened area.

The energy criteria used for delamination does not differentiate between compressive and tensile stresses and the through-thickness stresses are not considered where shell elements are concerned. However, the in-plane stress predictions used in the energy equation are affected by the number of elements through the thickness. Figure 17 shows the delamination through the thickness for the quarter plate model FE analysis fine9.

The delamination for analyses fine9 and fine2 is shown in Figs. 18 and 19. For both analyses the area of delamination is shown to be greatest for the RR-layer

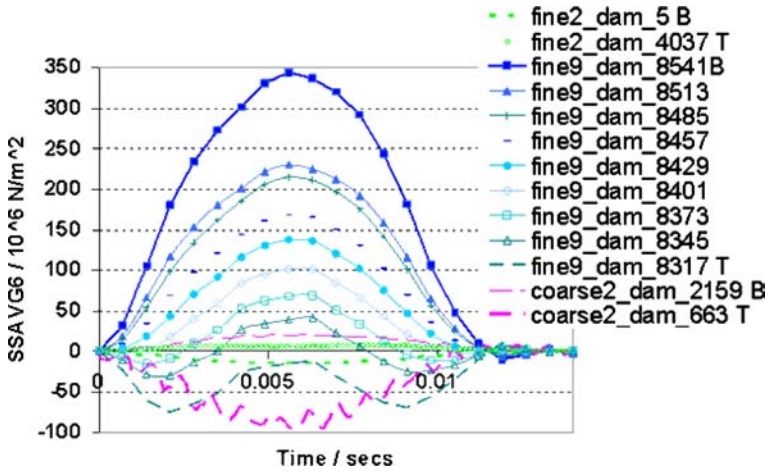

Fig. 14 The average normal transverse stress versus time, SSAVG6 for FE analyses modelling damage

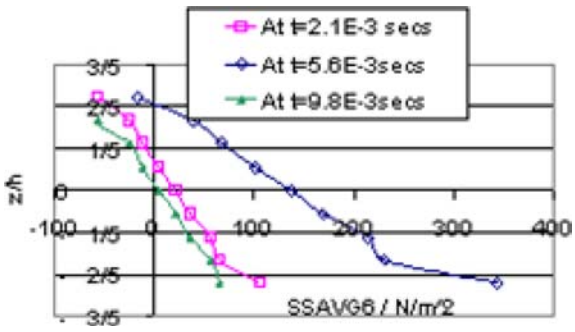

Fig. 15 SSAVG6 values from FE analysis ''fine9''

at the bottom of the plate, decreasing towards the centre of the plate and then increasing a little again towards the top surface. Analysis fine2 predicts delamination throughout the thickness, unlike fine9 showing damage on the top and bottom surfaces and two intact layers in the centre. Although the tests show delamination more extensively towards the top and particularly at towards the bottom of the plate, there is as yet no C-Scan data to assess the variation in the delamination seen in the FE results. What is known is that the maximum test delamination area at the bottom of the plate is more closely approximate by fine2 than fine9, whereas the opposite can be said about the maximum delamination within the top half of the plate. The number of elements through-the-thickness will affect the position of the eight RR-layers within the shell elements, thus outputting comparably varying in-plane stresses at the RR-layer integration points. Because the delamination model is one based on plane-stress, the amount of predicted delamination thus varies between models of varying through-thickness mesh densities. Table 6 shows a summary of test 9 results and the FE simulations of this test. In terms of

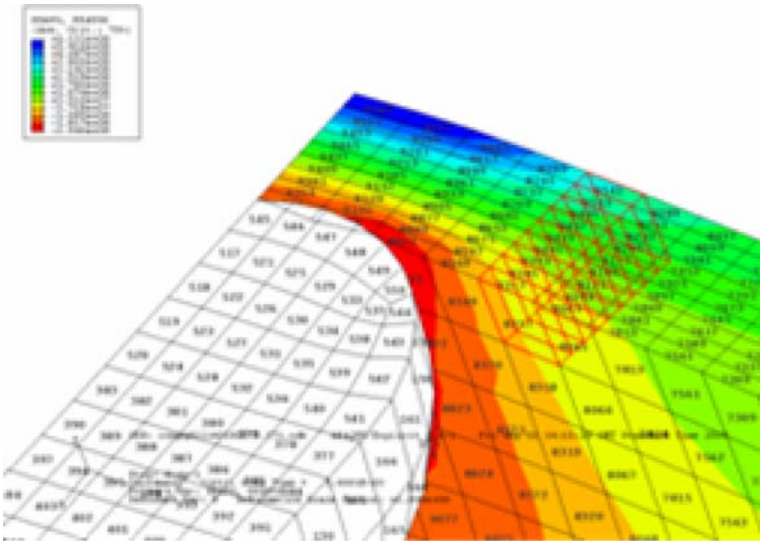

Fig. 16 SSAVG6 through the thickness at maximum o.o.p displacement for the analysis fine9, a quarter plate model

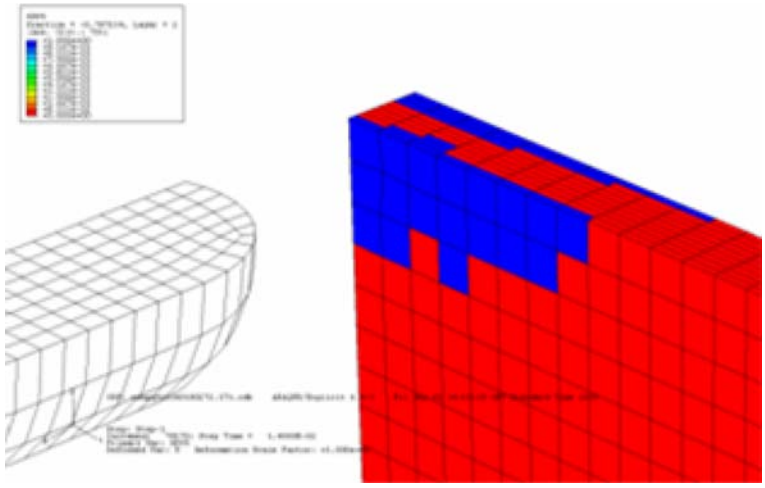

Fig. 17 Delamination through the thickness, analysis fine9

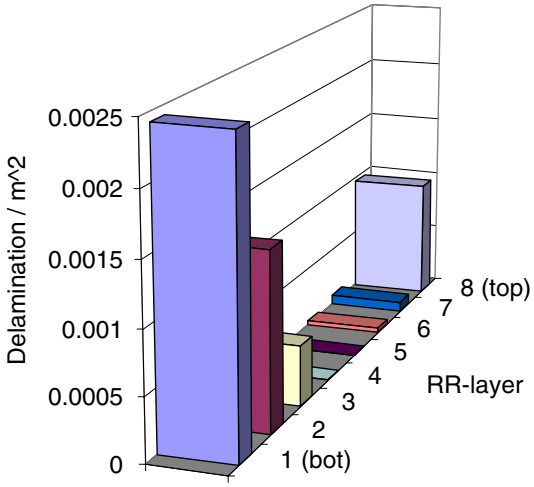

Fig. 18 Delamination damage through the thickness for FE analysis ''fine9''

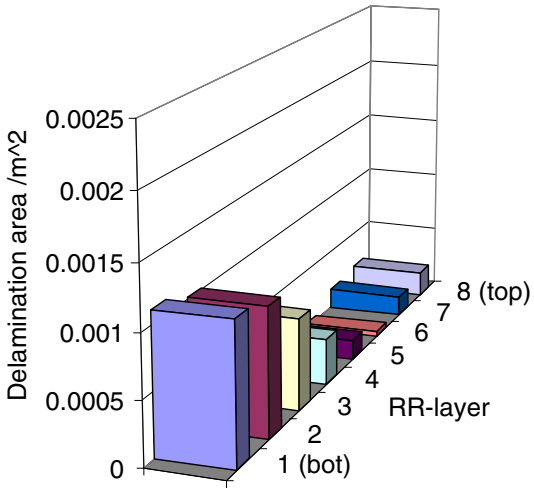

Fig. 19 Delamination damage through the thickness for FE analysis ''fine2''

Table 6 Summary of test 9 results and FE simulations of test 9

Analysis	Max o.o.p disp./m	Max. normal contact force/N	Max. SSAVG6 (ten. & com.)/ 10^6 N/m^{2a}	Delam. on bot. RR-layer/ 10^{-3} m^2
Coarse2	17.2	30.2	+19 –94	1.11
Fine2	17.3	28.2	6 –15	1.11
Fine9	16.68	29.9	350 –75	2.41
Test	15.3	26	–	1.45

[a] Maximum always on centre element, lower face

disp., displacement; ten., tension; com., compression; delam., delamination

the in-plane critical energy criterion used at the RR-layers, increasing the number of SC8R elements through the thickness does not increase the accuracy of the delamination damage predictions at these layers.

The in-plane density of the mesh has no significant effect on the delamination predictions through the thickness and the same delamination area is predicted at the bottom of the plate for coarse2 and fine2 analyses, see Fig. 20(i) and (ii). However, the maximum through-thickness stresses are noticeably affected, as seen with ''fine2'' and ''coarse2'' in Fig. 14. The delamination damage for the three different mesh analyses is shown for the RR-layer at the bottom face of the plate for test9 with Fig. 20(i–iii).

Test results of delamination damage at the top and bottom faces of the plates for tests 1, 3, 9 and 13 are shown in Table 7 together with their FE simulations carried out using a $56 \times 72 \times 2$ element mesh. Maximum delamination damage is captured relatively well, although slightly under-predicted again particularly at

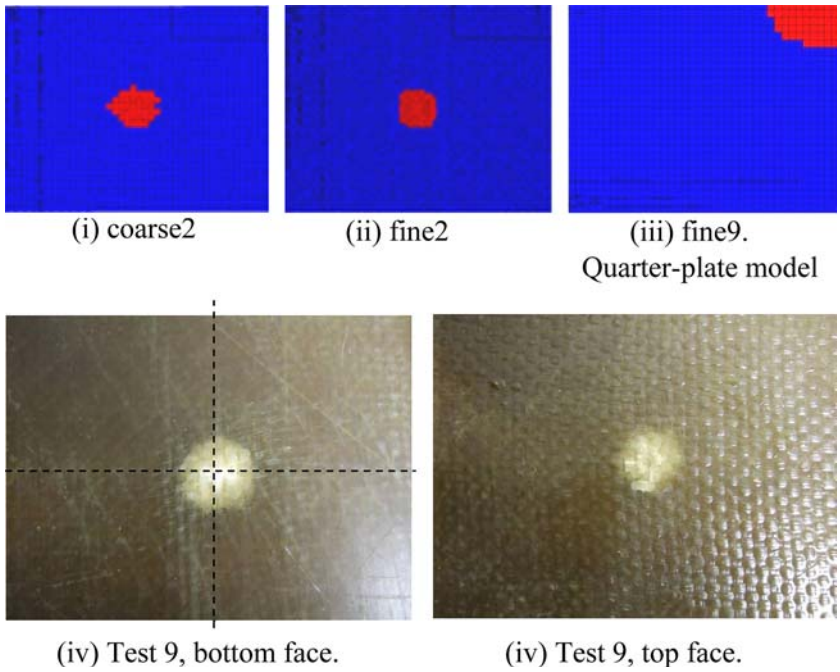

Fig. 20 (**i–iii**) FE analyses, showing delamination damage after impact at the bottom face of the plate, (**iv**) test 9 results for the bottom face, (**v**) test 9 results for the top face

Table 7 Delamination results for tests 1, 3, 9 and 13 and damage prediction from their respective FE simulations

Test	Test, delamination area/m (in)	FE, delamination area/m (in)	FE, matrix damage area/m (in)	FE, fibre damage area/m (in)
1	BOT: 0.0381 × 0.0381 (1.5 × 1.5) TOP: 0.0381 × 0.0254 (1.5 × 1)	0.0286 × 0.032 (1.125 × 1.245) TOP: zero	BOT: 0.04445 × 0.060325 (1.7499 × 2.375)	BOT: 0.05715 × 0.03175 (2.25 × 1.25)
3	BOT: 0.0381 × 0.0381 (1.5 × 1.5) TOP: 0.03175 × 0.0254 (1.25 × 1)	BOT: 0.03175 × 0.03175 (1.25 × 1.25) TOP: 0.0127 × 0.0127 (0.5 × 0.5)	BOT: 0.057 × 0.073 (2.24 × 2.87) TOP: 0.035 × 0.058 (1.38 × 2) Note: Not included is damage at corners	BOT: 0.057 × 0.0381 (2.24 × 1.5) TOP: 0.0381 × 0.016 (1.5 × 0.63)
9	BOT: 0.0381 × 0.03175 (1.5 × 1.25) TOP: 0.03175 × 0.0254 (1.25 × 1)	BOT: 0.03175 × 0.04445 (1.249 × 1.748) TOP: 0.0127 × 0.0159 (0.5 × 0.63)	BOT: 0.0635 × 0.0889 (2.5 × 3.5) TOP: large cross shape from corners	BOT: 0.07 × 0.057 (2.76 × 2.24) TOP: 0.0381 × 0.019 (1.5 × 0.75)
13	BOT: 0.0381x 0.0381 (1.5 × 1.5) TOP: 0.05715 × 0.03175 (2.25 × 1.25)	BOT: 0.04445 0.04445 (1.75 × 1.75) TOP: 0.015875 × 0.01905 (0.625 × 0.75)	BOT: 0.083 × 0.095 (3.27 × 3.74) TOP: large cross shape from corners	BOT: 0.073 × 0.07 (2.87 × 2.75) TOP: 0.0381 × 0.019 (1.5 × 0.75)

Top, top layer of plate; bot, bottom layer of plate

the top of the plate. Matrix and fibre damage on the other hand is substantially over-predicted in the FE analyses, with top layers appearing to suffer corner damage also, propagating towards the centre at the top ply. Generally we can say that Hashin's 2D failure criterion does not work satisfactorily in these simulations, producing unpredictable results.

Even for larger mass differences, simply increasing the mass of the tup will not generally increase the delamination area, as shown with tests1 and 2. Test 2 used a tup mass that was double that of test1. The delamination areas were the same but the extra impact energy in test 2 was expended in penetrating the plate. This was also proven for test 13 and test 12. In order to increase the delamination damage to the plates and prevent penetration, both the diameter and mass of the tup should be increased in the same test, as demonstrated through tests 15 and 16.

Photos of the damage incurred to the plates in tests 3 are taken for the bottom of the plate, see Fig. 21, shown together with its respective FE result. Delamination on the top and bottom face is shown in Fig. 22

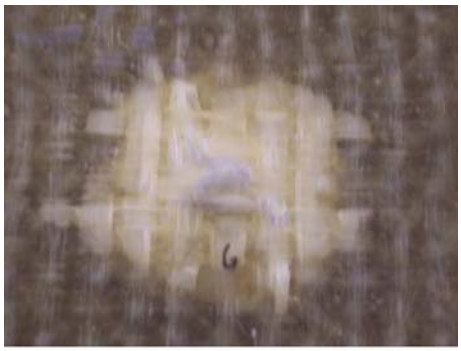

(i) Test 3, delamination bottom face

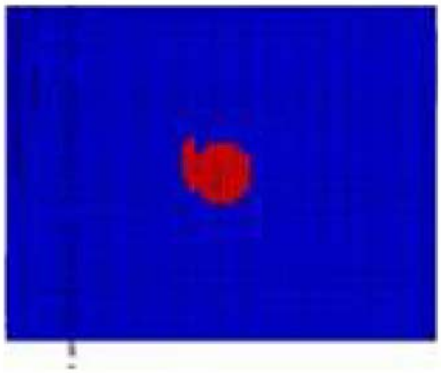

(ii)FE, delamination bottom face

Fig. 21 Delamination damage on the bottom face, (12.7 mm tup, 13.33 kg) (**i**) test 3, close-up of damage (**ii**) FE simulation of test

for test 13 and its FE simulation, and the delamination through the thickness is well captured in the FE model as shown with Fig. 23.

The o.o.p displacements at the centre of the plates impacted with the smallest tup, measuring 12.7 mm (0.5 in) in diameter are slightly over-predicted through the FE analyses by about 1 mm (0.04 in), shown in Fig. 24. However, the larger 38.1 mm (1.5 in) diameter tup with a larger mass, test 13, produced a maximum o.o.p displacement of nearly 23 mm, compared to the under-predicted 20 mm in the FE analysis.

The maximum contact force for Test 1 was measured as 15.5 kN compared to 19 kN in the FE analysis. Test 3 shows a maximum contact force of 20.35 kN, compared to 26.1 kN through FE. The largest difference between measured and predicted contact forces was for test 13; a 37% difference. All the other finite element analyses predict higher contact forces by up to 16% compared to experiment. However, the maximum contact force for the FE analyses are taken as the peaks of the contact force plots, which do see some oscillations. Taking instead, an average of the oscillations at peak contact, would bring the FE values down (see Fig. 25).

The tup in test 13 did not penetrate the plate but there was substantial damage in the form of delamination damage and matrix cracking on the bottom of

Fig. 22 Delamination damage Test 13 and FE simulation (38.1 mm tup, 26.19 kg)

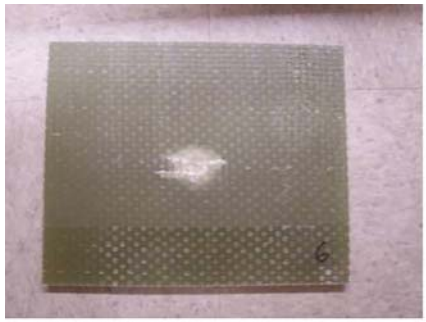

(i) Test 13, delamination top face

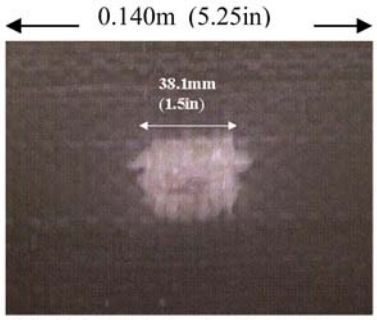

(iii) Test 13, delamination bottom face

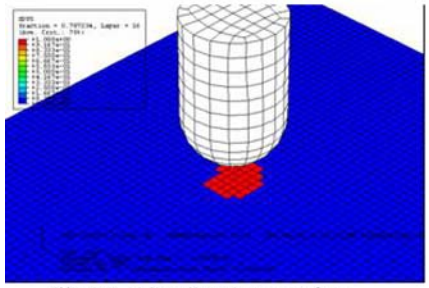

(ii) FE, delamination top face

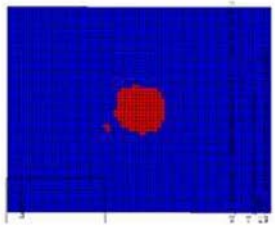

(iv) FE, bottom face

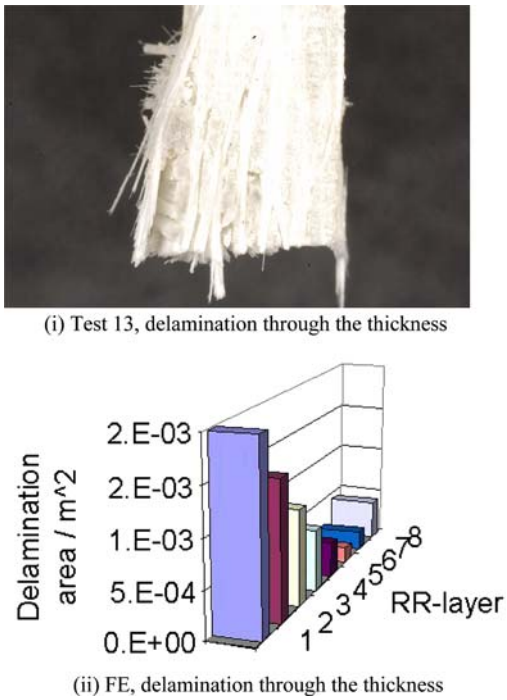

(i) Test 13, delamination through the thickness

(ii) FE, delamination through the thickness

Fig. 23 Delamination damage, Test 13 and FE (38.1 mm tup, 26.19 kg). (**i**) Through the thickness, test (**ii**) Through the thickness, FE

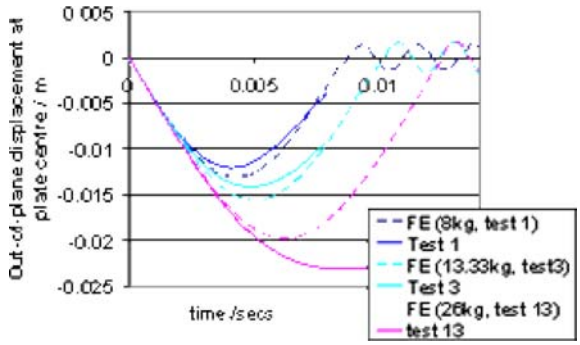

Fig. 24 Out-of-plane displacements at the plate centre versus time for tests 1, 3 and 13 and their FE simulations

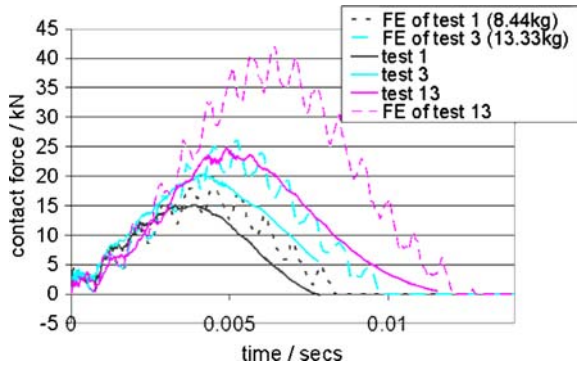

Fig. 25 Normal contact force versus time for tests 1, 3 and 13 and their FE simulations

the plate, with fibre failure occurring for some of the fibres in one or two bundles at the plate centre. However, the extent of matrix and fibre damage predicted with Hashin's criteria is again excessive. The in-plane damage modelled using the Hashin stress criteria was more extensive on the top and bottom layers only than in the test results, as shown with Fig. 26, but the effect is limited. Had the delaminated layers been physically modelled as separating, the FE o.o.p displacement would be larger and the contact force smaller. Although some of the stress will be carried by the membrane forces, the largest deformation (given the plate's width-to-thickness ratio and the simply supported boundary conditions) is in bending and transverse shear deformation. The transverse stiffness of the plate remains intact through-out the analysis therefore the FE analysis predicts that it is able to support more shear stress than in reality. The matrix damaged regions seen in Fig. 26 result in in-plane property degradation of that region which would only have a Poisson's effect on the change in thickness of the plate and will not affect the transverse strength, which may have been more damaged with the 38.1 mm (1.5 in) tup than with the smaller tups. This may be one reason why this test saw a proportionally larger over-prediction of the contact force and under-prediction of the o.o.p displacement compared to the smaller tup tests.

The cross-section of the plate in test3 after impact testing, corroborates the large effect of the tensile normal transverse stresses. The plate shows significant delamination near the bottom face of the plate where the tensile transverse normal stresses are acting to pull the plies apart. The top of the plate saw matrix crushing and some surface indentation, a characteristic witnessed in all the impact tests (see Fig. 27).

Conclusion

This work is aimed at modelling the shock loading response of large and small composite panels. The paper discusses a delamination model using resin-rich layers (RR-layers) that are modelled in between every ply.

The thick-shell and resin-rich layer (RR-layer) model can be applied to any composite and relies on a failure criterion at the RR-layers to depict delamination failure between two plies. The simple energy criterion at the RR-layers provides better results over the two simple stress criteria also tested. Here the energy value for failure requires the knowledge of the contact force; an empirical derivation chosen to

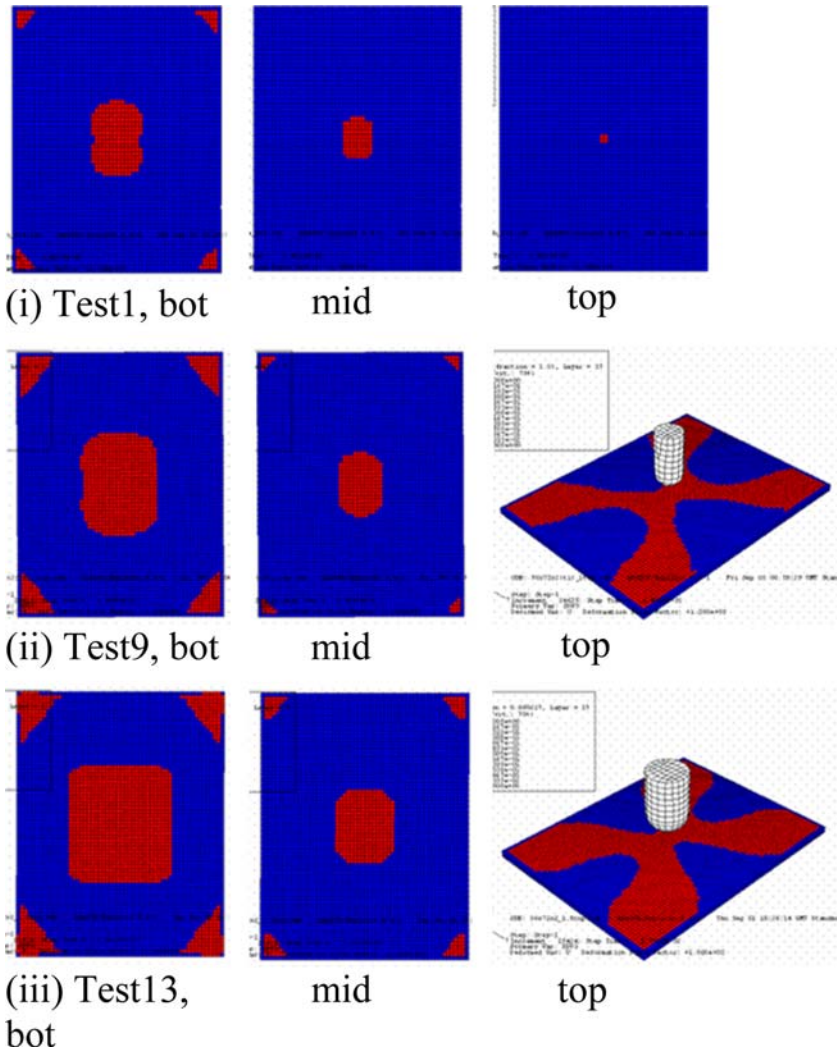

Fig. 26 Matrix cracking on the bottom, middle and top layers of test1, 9 and 13 FE simulations

Fig. 27 Cross-section of the plate in test 6 (12.7 mm, 16 kg), showing delamination on the back face

minimize the errors in the assessment of the resin-rich layer and energy concept. The method for obtaining an expression for this energy that is independent of each test is outside the scope of this work. What we can surmise is that the critical fracture energy value obtained from full-scale impact tests was relatively successful in this model unlike the value obtained from mode I fracture tests.

The delamination predictions obtained from all the impact test simulations are encouraging but ideally a 3d energy criterion is required. However, the main advantage of this 2d energy criterion for delamination is that it can be applied to shell elements and still obtain a reasonable prediction of the maximum delamination size. The criterion is also simple and quick to use and for the meshes tested is little affected by in-plane mesh density.

The density through the thickness (i.e., the number of stacked elements) is particularly influential on the through-thickness stress predictions and to a lesser extent on the in-plane stresses. For the meshes tested, the mesh density appears to have a negligible effect on the contact force, provided that the relative mesh size between the tup and the mesh are adequate.

The fibre and matrix damage predictions are not so agreeable. Hashin's 2d stress criteria in the prediction of these two damage modes is not reasonable or consistent between tests. The matrix damage for the large plates (which have clamped boundary conditions), is possibly a little under-predicted yet the fibre damage does not occur as extensively as predicted. The smaller, simply supported plate simulations show overly large areas of both damage modes.

The out-of-plane displacements obtained from the FE analyses on the small plates are all very conservative and this may be improved with a strain rate model. The ability to model the rate dependency of the material in the transverse direction could make a substantial difference to the FE results with regard to the out-of-plane stresses and strains. Using layered 3D solid (brick) elements could be one potential solution, however unlike Abaqus/Standard in Abaqus/Explicit the facility for layering currently does not exist.

There are restrictions in Abaqus/Explicit that prevent the efficiency of damage modelling of plate structures. The continuum shell elements are new to Abaqus; they can be stacked and appear to provide good normal transverse force predictions. However, the transverse force and stress estimates can be outputted but cannot be used in any subroutine, thus limiting the practicality of the SC8R element and preventing the implementation of a 3D failure criterion. In addition, only the in-plane material properties can be degraded as there is no control over the through-thickness moduli. Although the continuum shells have their advantages over thick shell elements they have yet to be further developed and they are currently of limited practicality in failure modelling.

Acknowledgements The authors are grateful for the financial support provided by the Office of Naval Research, Office of Naval Research Global and the Health and Safety Executive of the United Kingdom. This work is declared a work of the U.S. Government and is not subject to copyright protection in the United States.

References

1. Hinton MJ, Kaddour AS, Soden PD (2004) Failure criteria in fibre reinforced polymer composites: the world-wide failure exercise, a composites science and technology compendium. Elservier
2. Tang X, Shen Z, Chen P, Gaedke M (1997) Methodology for residual strength of damaged laminated composites. AIAA-97-1220
3. Elder DJ, Thomson RS, Nugen MM, Scott ML (2004) Composite Struct 66:677
4. Espinosa HD, Dwivedi S, Lu HC (2000) Compt Methods Appl Mech Engrg 183:259
5. Ruiz C (1986) Scaling in Penetration and Perforation Mechanics, Size Effects in Fracture, Farnborough, UK, 10th Nov 1986. pp. 11–16
6. Mines RAW, Roach AM, Jones N, Cantwell W (1999) Impact and residual properties of composite laminates subjected to secondary blast damage, Impact Research Centre. The University of Liverpool
7. Sutherland LS, Guedes Soares C (2005) Int J Impact Engrg 31:1
8. Davies GAO, Hitchings D (1996) Composites Part A 27A:1147
9. Kuboki T, Jar P-YB, Forest TW (2003) Comps Sci Tech 63:943
10. Hou JP, Petrinic N, Ruiz C (2001) Comps Sci Tech 61:2069
11. Reis L, de Freitas M (1997) Composite Struct 38:509
12. Johnson AF, Simon J (2001) Composites Part A 32:1197
13. Sun CT (2002) Modelling high strain rate response and failure in polymeric composites. The 2nd Int. Conf. On Struc. Stability and Dynamics, Dec. 16–18, 2002, Singapore
14. Khan AS, Huang S (1995) Continuum theory of plasticity. John Wiley & Sons Inc
15. Rajbhandari SP, Scott ML, Thomson RS, Hachenbeg D (2002) An approach to modelling and predicting impact damage in composite structures. ICAS Congress
16. Boh JW, Louca LA, Mouring SE (2005) Composites Part B 36:427
17. Lesar DE (2003) Composite sail advanced project report, plan for sensitivity analyses of rate-dependent composite material properties in composite advanced sail structure. NSWCCD 652
18. Greenfield RJ (1997) Dynamic tensile properties of woven glass fabric composites. Masters Thesis, University of Delaware
19. Jones N, Wierzbicki T (1993) Structural crashworthiness and failure. Elsevier Applied Science
20. Abaqus Analysis Users Manual, version 6.4. (NOTE: This is a reference manual for the finite element software Abaqus)